Cement & Concrete Composites 30 (2008) 788–797

Contents lists available at ScienceDirect

Cement & Concrete Composites

journal homepage: www.elsevier.com/locate/cemconcomp

Identification of concrete fracture parameters through size effect experiments

Luigi Cedolin [a], Gianluca Cusatis [b,*]

[a] Department of Structural Engineering, Politecnico di Milano, Milan, Italy
[b] Department of Civil and Environmental Engineering, Rensselaer Polytechnic Institute, Troy, NY 12180-3590, USA

ARTICLE INFO

Article history:
Received 25 January 2008
Received in revised form 21 May 2008
Accepted 25 May 2008
Available online 6 June 2008

Keywords:
Size effect
Cohesive crack law
Fracture energy
Tensile strength
Concrete
Mode I fracture
Experiments
Parameter identification

ABSTRACT

This paper deals with the identification of concrete fracture parameters through indirect methods based on size effect experiments. These methods utilize the size effect curve (structural strength versus structural size), associated with a certain specimen geometry, to identify the tensile strength and the initial fracture energy. These two parameters, in turn, are typically used to characterize the peak and the initial post-peak slope of the cohesive crack law. In the literature, two different approaches can be found for the calculation of the size effect curve: (a) an approach based on the polynomial interpolation of numerically calculated structural strengths of geometrically similar specimens of different sizes, and (b) the classical approach based on equivalent elastic fracture mechanics, which gives rise to the well-known Bažant's size effect law (SEL). In this paper, the two approaches are first reviewed, the relationship between them is investigated, and a new procedure to identify the tensile strength using the SEL is proposed. Then several sets of experimental results, recently performed at the Politecnico di Milano, are analyzed with both approaches in order to assess their range of applicability and accuracy in the identification of the two fracture parameters specified above.

1. Introduction

Fracture propagation in concrete is characterized by a dissipative zone, located at the crack tip and called the fracture process zone (FPZ), whose size is not negligible compared to usual structural sizes. Consequently, linear elastic fracture mechanics (LEFM) does not apply and the behavior of the FPZ needs to be simulated directly. For this purpose several mathematical and numerical models with various degrees of complexity can be found in the literature (for a comprehensive review see [1]). The simplest available model is the cohesive (or fictitious) crack model, pioneered for concrete by Hillerborg et al. [2]. Such model simulates the FPZ as an already formed ("fictitious") crack whose adjacent surfaces can still transmit stresses due to the crack bridging effect of material heterogeneities (aggregate pieces in concrete). These *bridging* (*cohesive*) *stresses* σ, in turn, are assumed to be a monotonically decreasing function of the *crack opening displacements* w in the FPZ. The bulk material outside the FPZ is assumed to behave elastically.

The stress versus crack opening relationship, also known as cohesive law or softening curve (Fig. 1b), interprets the behavior of a tensile specimen (Fig. 1a) as follows. The stress at $w = 0$ (incipient opening) represents the *effective* tensile strength f_t of the material and it is usually used to define crack initiation. The area under the curve (*total fracture energy*, G_F) represents the energy dissipated during the complete separation (formation of stress-free surfaces) of a unit area of concrete. The area under the initial tangent of the softening curve (*initial fracture energy* G_f, white circles in Fig. 1b) is a fraction of the total fracture energy which, as we will see, plays a significant role in the calculation of the failure load of test specimens [3]. Although various σ–w relationships have been adopted in the past, a bilinear law with an initial steep slope followed by a tail with mild inclination (Fig. 1b, white and black triangles) is currently favored in the fitting of experimental data.

Numerous experimental investigations carried out in the past have qualitatively corroborated the aforementioned Hillerborg's model and they clearly indicate that (see also Fig. 1a): (a) there exist a modest pre-peak nonlinearity, due to diffused microcracking preceding crack formation; (b) the peak stress, at which the fracture process starts to localize into a discrete crack, is larger than the tensile strength measured by direct tensile tests; (c) the initial and final parts of the softening curve are close to straight lines characterized, however, by very different inclinations.

Nevertheless, the experimental quantitative identification of the complete cohesive crack law is still a challenge and poses serious difficulties. Direct tension tests on unnotched specimens give rise to non-uniform strain and stress distributions both along the cross section and along the longitudinal axis [4]. This precludes the possibility of obtaining a real material law from the force per unit area versus average strain measurements. Measurements of the local displacement field around a propagating crack through

* Corresponding author. Tel.: +1 518 276 3956; fax: +1 518 276 4833.
E-mail address: cusatg@rpi.edu (G. Cusatis).

0958-9465/$ - see front matter © 2008 Elsevier Ltd. All rights reserved.
doi:10.1016/j.cemconcomp.2008.05.007

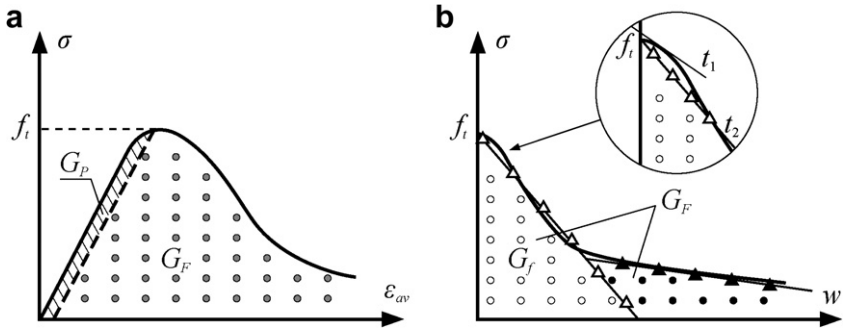

Fig. 1. (a) Stress–elongation curve in an uniaxial tensile test of concrete. (b) Stress–crack opening displacement curve.

optical interferometry with laser light would allow the determination of the cohesive law [5], but this procedure is far too sophisticated for practical applications. The identification of the entire softening curve through an inverse analysis of the complete load versus displacement curve of notched specimens is also affected by numerical and experimental difficulties [1,6–8,22].

More promising appears the identification of the initial part of the softening curve, characterized by the tensile strength f_t and the initial fracture energy G_f, through the analysis of the experimental peak loads of specimens of the same geometry but different sizes (*size effect*). This procedure avoids the difficulties associated with the measurement of the softening branch of specimen response and it is motivated by the finding that, at least within a certain range of specimen characteristic sizes, only the initial part of the softening curve is relevant to the structural performance (*structural strength*) [8]. Under these circumstances, the identification of f_t and G_f can be carried out through the use of the *cohesive crack size effect law* (CCL), in which the structural strength versus structural size can be readily calculated through finite element analysis based on a linear cohesive crack law [8]. The size effect identification of f_t and G_f can be also carried out by adopting [1,9–12] Bažant's *size effect law* (SEL), which was derived from equivalent linear fracture mechanics concepts and without any reference to Hillerborg's cohesive model.

The use of CCL and SEL for studying size effect and, in particular, for identifying the fracture parameters, has been widely accepted among researchers and both of them have been extensively used [1,3,9–11]. Nevertheless, there is still a lack of understanding of (a) their mutual relationship, (b) the accuracy of the fracture parameter identification by using the CCL and the SEL, and (c) the range of applicability of both methods.

This paper reports on the findings of a recent experimental and computational research program carried out at the Politecnico di Milano with the aim of clarifying the aforementioned open issues. Additional references to the obtained results can be also found in [11].

2. Size effect

2.1. Cohesive crack size effect law (CCL)

Since our attention will be focused on the structural strength (peak load) of laboratory specimens, for which the stress distribution in the fracture process zone shows stress values normally belonging to the initial part of the softening curve, we will make reference to a *linear* cohesive crack law, characterized by the effective tensile strength f_t and initial fracture energy G_f (Fig. 2b).

Considering a certain specimen geometry, it is possible, through the use of appropriate numerical methods (e.g., the finite element method), to calculate for any characteristic dimension D (Fig. 2c) of the specimen the corresponding nominal stress σ_N at the peak load (ultimate nominal stress or structural strength). For the case of a linear cohesive crack law, Planas et al. [13] have shown that the stress σ_N can be expressed through a function ψ which depends uniquely on the ratio D/l_1, i.e.

$$\sigma_N = f_t \psi(D/l_1) \tag{1}$$

in which $l_1 = EG_f/f_t^2$ is the *characteristic length* related to the *initial* fracture energy and E is Young's modulus of the material. The function ψ depends on the geometry of the specimen and can be obtained through a polynomial interpolation of numerical results.

The CCL can be also rearranged in the form

$$\frac{f_t^2}{\sigma_N^2} = [\psi(D/l_1)]^{-2} \tag{2}$$

which, in the plane $Y = (f_t/\sigma_N)^2$ and $X = D/l_1$, is represented by a curve featuring an inclined asymptote (see Fig. 2a, the curve with white triangles). Since (as we will see) the SEL is represented in the same plane by a straight line, if both approaches are considered valid for the interpretation of experimental test results the SEL and the CCL asymptote must coincide [9].

The best fitting of the experimental results (relevant to peak loads of geometrically similar specimens) on the basis of Eq. (1) or Eq. (2) leads to the identification of f_t and G_f (and consequently l_1). Note that, since Eqs. (1) and (2), are nonlinear, the best fitting must be performed through a nonlinear optimization algorithm.

At the peak load the material in the softening regime reaches the tail of the softening curve only for large enough specimens. Consequently, the function ψ calculated on the basis of a linear cohesive crack law can only be used to model the structural strength of small to medium size specimens (where "small", "medium", and "large" indicate how specimen characteristic sizes D relate to the material characteristic length l_1). For large specimens the structural strength is influenced by the tail, and consequently the CCL curve deviates from the asymptote as shown by the black triangles in Fig. 2a.

2.2. Bažant's size effect law (SEL)

The size effect on structural strength of quasi-brittle materials such as concrete, cannot be described through the classical *linear elastic fracture mechanics* (LEFM) because these materials are characterized by a *fracture process zone* (FPZ) length l_{FPZ} (Fig. 2c) that is large compared to the characteristic size D of the structure. In this case, however, fracture and size effect can be modeled [1,14] through the use of the equivalent linear elastic fracture mechanics, in which LEFM equations are used with reference to an equivalent crack which consists of the actual stress-free crack (sharp notch or preexisting fatigued crack) plus a finite length c_f (critical equivalent crack extension or simply crack extension) associated with the size of the FPZ (Fig. 2c).

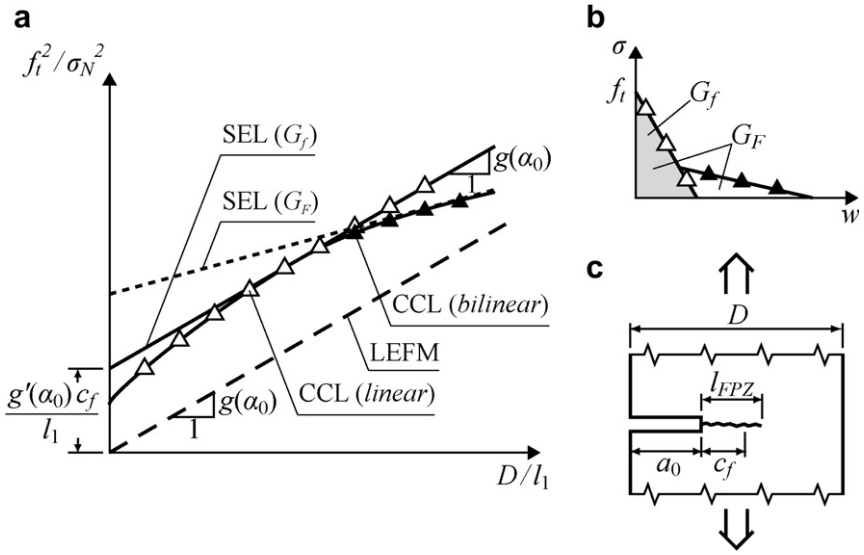

Fig. 2. (a) Size effect law. (b) Bi-linear cohesive crack law. (c) Definition of the fracture process zone length and of the crack extension.

Considering specimens of the same geometry, different sizes and notch length $a_0 = \alpha_0 D$, the introduction of the concept of an effective crack of length $a_0 + c_f$ into the LEFM equation for the nominal stress at failure gives $\sigma_N = K_c/[Dg(\alpha_0 + c_f/D)]^{1/2}$ (K_c = critical stress intensity factor). The subsequent Taylor expansion of the dimensionless LEFM energy release function $g(\alpha_0 + c_f/D) \approx g(\alpha_0) + g'(\alpha_0)c_f/D$ (with retention of only the first term of the expansion) [14] leads to the well-known SEL $\sigma_N = K_c/[Dg(\alpha_0 + c_f g'(\alpha_0)]^{1/2}$, in which c_f must be regarded as a constant independent of the size D. By using the classical Irwin's equation $K_c^2 = EG_f$, with reference to the initial fracture energy G_f, the SEL can be rearranged in the form

$$\frac{1}{\sigma_N^2} = \frac{g(\alpha_0)}{EG_f} D + \frac{g'(\alpha_0)c_f}{EG_f} \tag{3}$$

The use of the initial fracture energy in the framework of the equivalent LEFM may seem questionable since this theory implicitly assumes a fully developed FPZ characterized by a vanishing cohesive stress at the tip of the stress-free crack. Indeed, such hypothesis would require the use of the total fracture energy G_F instead of G_f. However, as it will be verified later in this paper, the SEL associated with G_f, coincides with the asymptotic response shown by the CCL. Since, in most of the situations, the convergence of the CCL to the asymptote is very fast, the SEL associated with G_f is regarded here as an accurate approximation of the CCL (at least in a certain range of sizes, Fig. 2a) more than representative of the real behavior of large structures. Consequently, the SEL can be seen as a valid alternative to the CCL for the identification of G_f and f_t on the basis of size effect experiments, with the advantage that (a) it requires only a linear regression analysis of experimental data as opposed to the nonlinear optimization required by the CCL, and (b) it embeds the effect of different specimen shapes and boundary conditions through the dimensionless energy release function $g(\alpha)$.

The fitting of size effect experimental data (maximum loads of specimens of the same geometry but of different sizes) on the basis of Eq. (3), performed with a linear regression, leads to the determination of the coefficients a and c of the straight line $y = ax + c$ in the plane $y = (1/\sigma_N)^2$ and $x = D$. From these coefficients the values of the fracture energy $G_f = g(\alpha_0)/Ea$ and of the crack extension $c_f = cg(\alpha_0)/ag'(\alpha_0)$ can be calculated. The value of G_f is inversely proportional to the slope a and the crack extension c_f is proportional to the intercept at the origin c.

Furthermore, if the equivalent crack extension c_f is proven to be a material property, it is possible to establish a unique relationship between c_f and the parameters of the cohesive law. As verified in the following, c_f is proportional to the characteristic length l_1 and the coefficient of proportionality is approximately constant regardless of specimen shape and boundary conditions (a similar result was obtained in [7]).

In order to exploit the previously mentioned equivalence between the SEL and the asymptotic behavior of the CCL it is useful to multiply both sides of Eq. (3) by the square of the tensile strength f_t, and to rewrite the SEL as follows:

$$\frac{f_t^2}{\sigma_N^2} = g(\alpha_0)\frac{D}{l_1} + g'(\alpha_0)\frac{c_f}{l_1} \tag{4}$$

which is a straight line of slope $A = g(\alpha_0)$ and intercept at the origin $C = g'(\alpha_0)c_f/l_1$ in the plane $Y = (f_t/\sigma_N)^2$, $X = D/l_1$ (Fig. 2a). Eq. (4) shows that (a) the SEL coincides with the asymptote of the CCL if the slope of such asymptote is equal to the dimensionless energy release rate $g(\alpha_0)$, and (b) the equivalent crack extension c_f is a material property if the intercept of the asymptote of the CCL divided by the derivative of the dimensionless release rate $g'(\alpha_0)$ is constant and independent on specimen shape and boundary conditions.

3. Numerical simulations

In order to verify the equivalence between the SEL and the asymptotic behavior of the CCL, several numerical simulations were performed using a finite element code in which the cohesive crack law is implemented through the use of zero-thickness interface elements [15]. The mesh was refined in the region (Fig. 3b) of crack propagation, enabling both an accurate representation of the stress profile in the FPZ and a precise determination of the maximum load.

Three kinds of tests were considered (Fig. 3c): three-point bending (TPB), single notch traction (SNT) and double notch traction (DNT). The specimens were rectangular plates (Fig. 3a) having thickness $B = 80$ mm, depth $D = 60$, 120, 240, 480, 720, 960, 1440, 1920, and 3840 mm, length $S = 4D$, and notch length $a_0 = \alpha_0 D$, with $\alpha_0 = 0.3$. For all sizes, the notch was kept of constant width (3 mm) and constant curvature at the tip. The values adopted for the mechanical properties of the material were $E = 30{,}000$ N/mm^2,

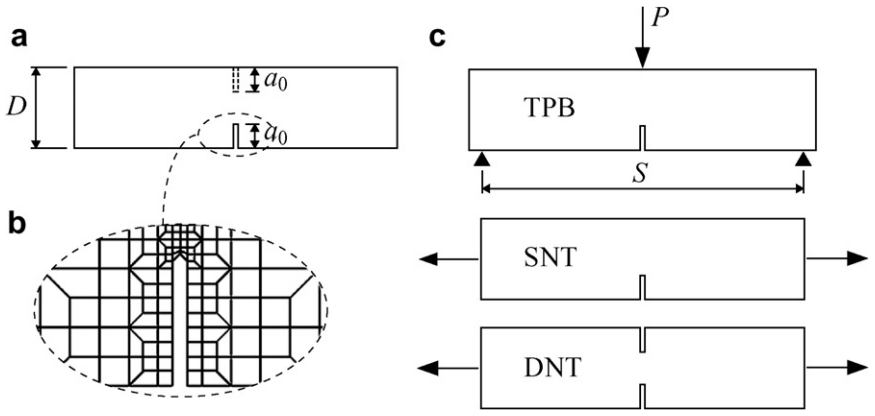

Fig. 3. Typical (a) notched specimen geometry, (b) finite element mesh resolution, and (c) boundary conditions considered in the simulations.

$\nu = 0.2$, $f_t = 3$ N/mm^2, $G_f = 0.030$ N/mm (linear softening), $l_1 = EG_f/f_t^2 = 100$ mm.

For the TPB specimens, the finite element calculations [16] yielded, for every depth D, the nominal stress at failure $\sigma_N = 3P_{max}S/(2BD^2)$ and the stress distribution along the ligament (Fig. 4a), from which the length of the fracture process zone l_{FPZ} and the tensile stress at the tip of the notch σ_{tip} (Fig. 4c and d, respectively) could be determined.

The plot of $Y = (f_t/\sigma_N)^2$ as a function of $X = D/l_1$, reported in Fig. 4b, shows the presence of an asymptote which may be accurately represented by the straight line which connects the farthest two calculated points of the curve, expressed by $Y = A^*X + C^*$, with $A^* = 1.021$ and $C^* = 2.036$. Since the value of A^* is practically coincident with the value $A = g(\alpha_0) = 1.0247$ reported in [17] for TPB specimens, the comparison with Eq. (4) indicates that the asymptote of the CCL coincides with the SEL. This coincidence can be further exploited to calculate the value of the crack extension $c_f = C^* l_1/g'(\alpha_0) = 38.8$ mm (Eq. (4)).

Let us examine now the values of the FPZ length l_{FPZ} resulting from the stress distributions along the ligament (Fig. 4a) calculated using finite elements. Fig. 4c shows that l_{FPZ} increases with D/l_1 and reaches a horizontal asymptote given approximately by $l_{FPZ,\infty} = 68$ mm ($l_{FPZ,\infty} = 67.96$ mm for $D = 3840$ mm). The ratio $c_f/l_{FPZ,\infty} = 38.8/68 = 0.57$ is in line with the physical interpretation of c_f according to equivalent linear elastic fracture mechanics [1].

Fig. 4d shows that the stress at the notch tip decreases with D/l_1, reaching a value of $\sigma_{tip}/f_t = 0.05$ for $D = 3820$ mm, which indicates that the fracture process zone length has almost reached its asymptotic value. We must keep in mind, however, that the assumption of linear softening may at most be considered physically realistic down to values of about $\sigma_{tip}/f_t = 0.2$, which correspond to values of D/l_1 of around 5.8. For higher values of D/l_1 a

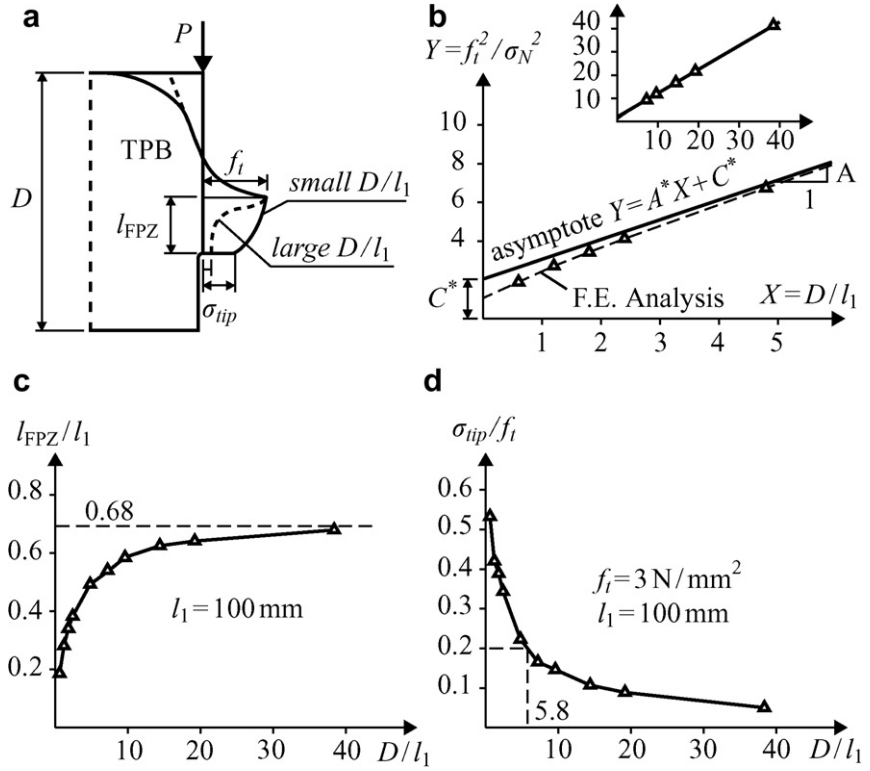

Fig. 4. (a) Typical stress profile in the FPZ. (b) CCL size effect curve and its asymptote. (c) Normalized FPZ length. (d) Normalized crack tip stress at the peak load.

Table 1
Calculated values for the CCL asymptote

	A^*	C^*	$g(\alpha_0)$	$g'(\alpha_0)$
TPB	1.021	2.036	1.024	5.246
SNT	2.602	8.020	2.590	19.64
DNT	1.184	1.469	1.190	3.988

Table 2
Calculated values for c_f and $l_{FPZ,\infty}$

	$l_{FPZ,\infty}$ (mm)	$l_{FPZ,\infty}/l_1$	c_f (mm)	c_f/l_1	$c_f/l_{FPZ,\infty}$
TPB	68	0.68	38.8	0.39	0.57
SNT	70	0.70	40.7	0.41	0.58
DNT	71	0.71	36.8	0.37	0.52

bilinear σ–w relationship would increase the value of l_{FPZ}, change the shape of the stress distribution in the FPZ (Fig. 4a), and make the curve $(f_t/\sigma_N)^2$ deviate from the asymptote for high values of D/l_1, as shown in Fig. 2a.

The numerical calculations have been also repeated [16] for single and double-notched traction specimens of the same dimensions (Fig. 3c). Tables 1 and 2 summarize the results obtained for all three types of loading.

From Table 1 it appears that there is a consistent agreement between the slope of the asymptote of the CCL (with linear softening) and the dimensionless release rate $g'(\alpha_0)$. Table 2 shows that the asymptotic values of the fracture process zone length $l_{FPZ,\infty}$ and of the equivalent crack extension c_f computed with the different loading conditions are remarkably close. Moreover, if one takes into account the influence of the finite element approximations on the determination of the maximum load and of the asymptote, we can consider the values obtained for the different geometries practically coincident and therefore regard them as material properties. The ratio between the crack extension c_f and the characteristic length l_1 is very close to the value (0.42) reported in [1] for linear softening.

The previous analysis confirms that a unique relationship exists between the SEL parameters (G_f, c_f) and the cohesive crack parameters (G_f, f_t). Such relationship can be used to calculate c_f on the basis of the cohesive crack parameters G_f and f_t. Conversely, it is also possible to compute the tensile strength from the SEL parameters G_f and c_f. If we assume from Table 2 $c_f = 0.39\, l_1 = 0.39\, EG_f/f_t^2$ we obtain the formula

$$f_t = (0.39 E G_f / c_f)^{1/2} \tag{5}$$

In the authors' knowledge, this is the first time that this procedure to identify f_t through the use of the SEL has been proposed and analyzed.

4. Experimental results

A series of experimental investigations have been conducted at the Politecnico di Milano with the purpose of evaluating the applicability of the SEL and of the CCL for the identification of the fracture parameters f_t and G_f of concretes with different compositions. The results reported here are relevant to the three-point bending (TPB) specimens obtained from four concrete batches, N [18], S [18], B [19] and C [20]. Their characteristics are summarized in Table 3.

The TPB specimens are characterized (Fig. 3a and c) by a ratio $S/D = 8/3$, $\alpha_0 = 0.3$, notch width 3 mm and thickness $B = 80$ mm. For concretes N, S and B the depths of the specimens are $D = 120$, 180, 240 mm, and the number of specimen tested for each size is $n = 3$, while, for Concrete C, $D = 120$, 200, 320 mm and $n = 4$ (Table 4). The loading rate adopted was $d\sigma_N/dt = 0.012$ N mm^{-2} s^{-1}. The mean values of σ_N at failure are reported in Table 4, together with their coefficient of variation ω.

4.1. Concrete N

As previously mentioned, the identification of the SEL parameters from the mean values in Table 4 can be done through a linear regression $y = ax + c$. One obtains $a = 0.001228$, $c = 0.09020$, from which $G_f^{SEL} = g(\alpha_0)/Ea = 0.0345$ N/mm and $c_f^{SEL} = cEG_f^{SEL}/g'(\alpha_0) = 14.35$ mm, $f_t^{SEL} = (0.39\ EG_f^{SEL}/c_f^{SEL})^{1/2} = 4.76$ N/mm^2, and $l_1^{SEL} = 36.78$ mm.

Let us analyze now the same results through the cohesive crack model (with linear softening), adopting as function ψ the expression proposed by Planas et al. [13] for three-point bending specimens (calculated for the given value of α_0)

$$\psi = \frac{\sigma_N}{f_t} = 1.47\left[\frac{1 + 3.843\sqrt{z}}{1 + 0.5651\sqrt{z}} + 2.2288 z\right]^{-\frac{1}{2}} \tag{6}$$

in which $z = D/l_1^{CCL}$. By adopting a least-square optimization algorithm, the best fitting of the experimental data of Table 4 through Eq. (6) gives $f_t^{CCL} = 4.23$ N/mm^2 and $G_f^{CCL} = 0.0367$ N/mm.

A graphical interpretation of the optimization procedure is given in Fig. 5. For the experimental values of σ_N corresponding to a certain size D, Eq. (6) defines an implicit relation between f_t and G_f, represented by a curve in the (f_t, G_f) plane (Fig. 5a). The points of interception of any two of these curves, which represent the solutions predicted by considering two sizes only, are far apart, while they coincide for the curves corresponding to the σ_N values

Table 4
Test results

Concrete mix	D (mm)	σ_N (N/mm^2)	ω (%)
N	120	2.07	6.15
	180	1.77	7.53
	240	1.62	3.35
S	120	2.50	2.46
	180	2.13	2.84
	240	1.98	4.75
B	120	2.69	1.84
	180	2.38	1.28
	240	2.22	3.56
C	120	2.67	4.47
	200	2.40	3.86
	320	2.16	5.56

Table 3
Concrete compositions and mechanical properties

Concrete mix	Aggregate		Cement content (kg/m^3)	w/c	E (N/mm^2)	f'_c (N/mm^2)
	Type*	d_a (mm)				
N	A	16	300	0.60	24200	28.5
S	C	16	570	0.44	28600	54.8
B	A	16	330	0.55	32680	33.7
C	A	16	380	0.50	28690	49.6

* A, alluvial; C, crushed.

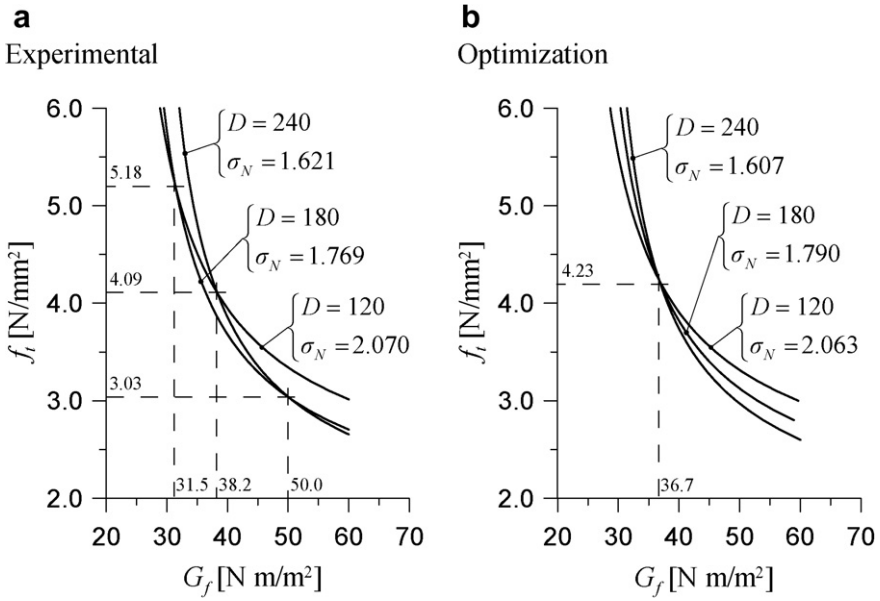

Fig. 5. (a) f_t–G_f curves based on experimental values of σ_N for concrete N. (b) Same as in (a), but using values of σ_N predicted by the model.

predicted by the model (Fig. 5b). From the values listed for σ_N in Figs. 5a and 5b, it appears that small variations of σ_N (i.e. of the peak load) give rise to substantial variations of G_f and f_t, thus indicating a high sensitivity of the identification process to the scatter of the experimental data. As pointed out by Planas et al. [3], this is related to the similarity of the slopes of the curves at their points of interception.

The identified CCL and SEL are shown in Fig. 6 as dashed and solid lines, respectively. Note that the two lines make reference to a different set of scales, chosen in such a way that the position of the test data points coincides in the two representations. If the agreement between the predictions of the two laws were perfect, the two scales would be exactly superimposed and the SEL would coincide with the asymptote of the CCL curve.

The results of the analysis of concrete N are summarized in Table 5. The difference between the identified values of the initial fracture energy and tensile strength (about 6% and 13%, respectively) appears to be totally acceptable.

4.1.1. Comparison with numerical results

Since the range of experimental values of D/l_1 (from 2.5 to 5.1 according to the CCL scale) is fairly well-represented by the results of the numerical simulations relative to the sizes $D = 2.4l_1$ and $D = 4.8l_1$ (Fig. 4b), it is interesting to calculate the values of G_f and c_f which would be predicted by a regression line passing through these points. One would obtain $G_f' = 0.0282$ N/mm and $c_f' = 27.17$ mm, with an error of around −6% for G_f and −29% for c_f with respect to the values obtained from the asymptote. These values are comparable to the discrepancies appearing from Table 5. It must be also noted that the largest experimental ratio D/l_1 (5.14) belongs to a range (Fig. 4d) in which the stress at the notch tip could lie on the tail of the softening curve, justifying the slight deviation from the linearity of the third experimental data point.

The length of the fracture zone may then be estimated as $l_{FPZ,\infty} = (1/0.6)\, c_f \approx 30$ mm, a value which may seem smaller than expected. We must keep in mind, however, that this prediction comes from the initial fracture energy and not from the total fracture energy.

From a physical point of view $l_{FPZ,\infty} = 30$ mm corresponds roughly to twice the maximum aggregate size. A possible interpretation of this result can stem from the meso-scale analysis of the

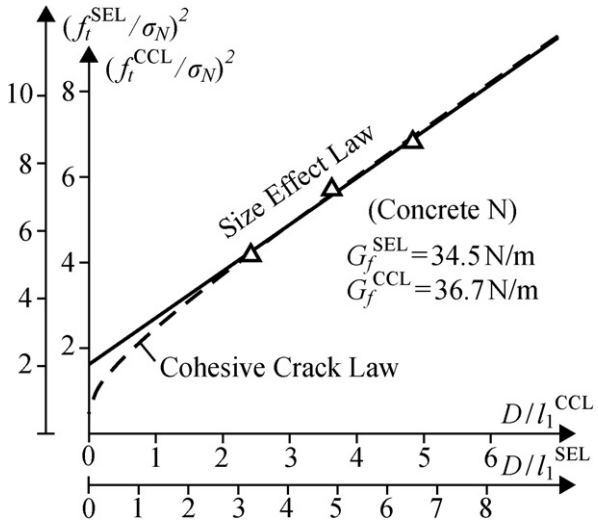

Fig. 6. Identified SEL and CCL for concrete N.

fracture process, through the use of a two-scale procedure and a meso-scale lattice model recently developed by the authors [21–24]. It has been shown [24] that the meso-scale fracture energy, used to reproduce the dissipation phenomena that occur in the matrix (cement paste and/or fine mortar) between coarse aggregate pieces, basically coincides with the initial fracture energy G_f. Meso-scale phenomena (and so the meso-level fracture energy) are necessarily associated with a meso-scale fracture process zone whose size can be reasonably assumed of the order of magnitude of the maximum aggregate size. As a consequence, it is reasonable to consider the crack extension c_f to be associated with this

Table 5
Values of identified parameters for concrete N

	G_f (N/mm)	c_f (mm)	f_t (N/mm²)	l_1 (mm)
SEL	0.0345	14.35	4.76	36.78
CCL	0.0367	19.36	4.23	49.64

meso-scale FPZ instead of the macro-scale FPZ, whose size is expected to be several times the maximum aggregate size.

4.2. Concrete S

The fitting of the test results using the SEL gives for the parameters of the linear regression $y = ax + c$ the values $a = 0.00079$ and $c = 0.06874$, which lead to the results reported in the first row of Table 6. The second row of Table 6 shows the results obtained through nonlinear optimization using the CCL.

The obtained CCL and SEL curves are shown in Fig. 7, from which it appears that the asymptote of the CCL curve differs slightly from the SEL. These results appear similar to those obtained for concrete N and so the same conclusions can be drawn.

4.3. Concrete B

The fitting of the test results through the SEL gives $a = 0.00079$ and $c = 0.06874$ and leads to the values of the fracture parameters reported in the first row of Table 7. The nonlinear optimization using the CCL leads the values listed in the second row of Table 7.

Table 7 shows that the agreement between the SEL and the CCL is poor. The differences between the identified initial fracture energy and tensile strength with the two methods are about 18% and 30%, respectively. The crack extensions and the characteristic lengths computed through the two methods differ of about 100%.

This disagreement appears also in Fig. 8 as a deviation of the SEL from the asymptote of the CCL, deviation which is clearly related to the low values of D/l_1 (below 2 on the CCL scale) that characterize the experimental results. This causes the SEL regression line to have a steeper slope than the CCL asymptote and consequently to predict a lower value for G_f.

Table 6
Values of identified parameters for concrete S

	G_f (N/mm)	c_f (mm)	f_t (N/mm^2)	l_1 (mm)
SEL	0.0453	16.99	5.45	43.56
CCL	0.0482	23.53	4.78	60.33

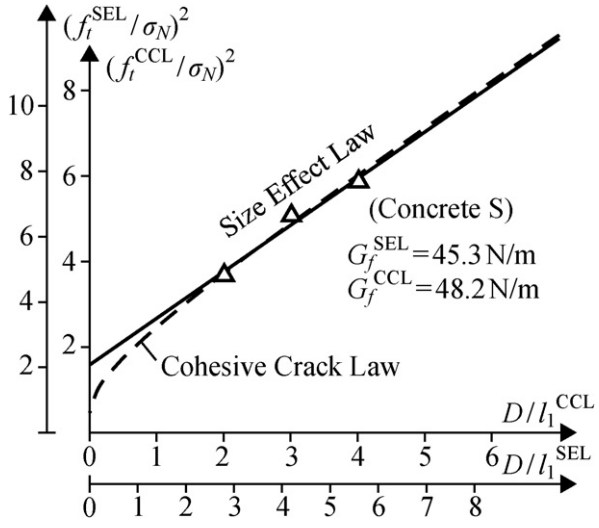

Fig. 7. Identified SEL and CCL for concrete S.

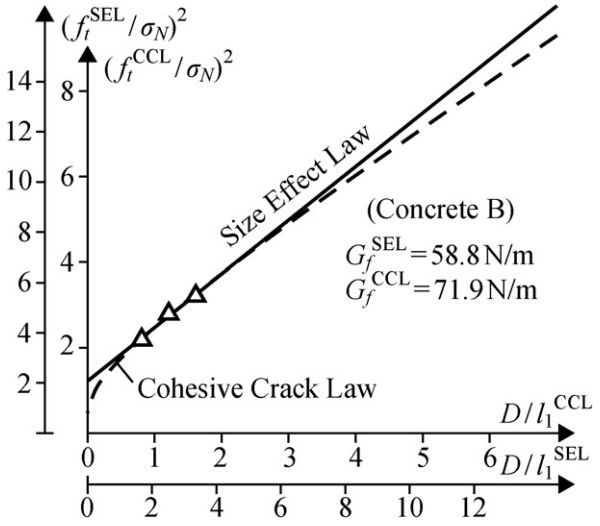

Fig. 8. Identified SEL and CCL for concrete B.

4.4. Concrete C

The fitting of the test results through the SEL gives $a = 0.000362$ and $c = 0.09875$ and leads to the values of the fracture parameters reported in the first row of Table 8. The nonlinear optimization using the CCL leads to the values listed in the second row of Table 8. Again, as in the case of the concrete B, the difference between the parameters identified through the two methods is large. The difference in terms of initial fracture energy and tensile strength is 35% and 48%, respectively. The characteristic length associated with the CCL is more than twice the one associated with the SEL.

As for concrete B, these discrepancies are explained by the low experimental values of D/l_1 (Fig. 9). It must be also noted that the values predicted for G_f by both the SEL and the CCL (0.098 and 0.152 N/mm, respectively, see Table 8) are clearly unrealistic for the given composition of concrete C.

It is important to point out that in this case the experimental results are particularly close to the predictions of the cohesive crack law, i.e. the three curves f_t–G_f (not shown) corresponding to the experimental σ_N have much closer interceptions than those appearing in Fig. 5a for concrete N. The scatter of experimental results, therefore, cannot be blamed for the discrepancies between the two models.

4.5. SEL versus CCL

The application of the two models to experimental data regarding TPB specimens of normal sizes (depth D in the range 120–300 mm) produced two distinct outcomes.

The first occurs for concretes N and S, for which the experimental ratios D/l_1 lie in an intermediate range (between 2 and 5 on the CCL scale) where the CCL curve is close to the asymptote and the SEL approximation is applicable. The values of the fracture

Table 7
Values of identified parameters for concrete B

	G_f (N/mm)	c_f (mm)	f_t (N/mm^2)	l_1 (mm)
SEL	0.0588	27.94	5.18	71.6
CCL	0.0719	58.14	3.97	149.1

Table 8
Values of identified parameters for concrete C

	G_f (N/mm)	c_f (mm)	f_t (N/mm^2)	l_1 (mm)
SEL	0.0986	53.27	4.55	136.6
CCL	0.1526	181.16	3.07	464.5

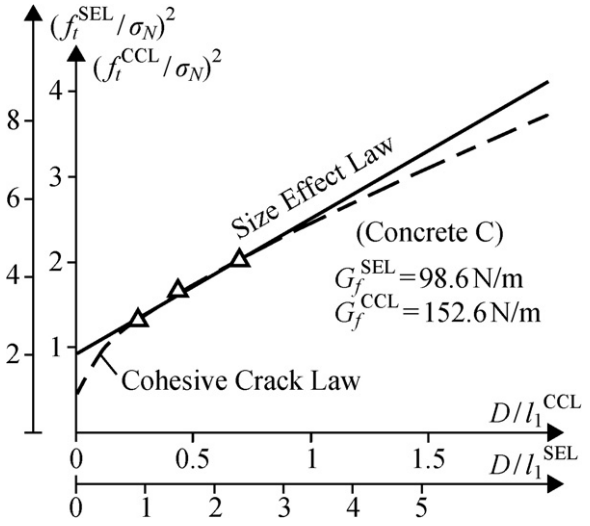

Fig. 9. Identified SEL and CCL for concrete C.

parameters predicted by the two models are sufficiently close and belong to an acceptable range.

The second is illustrated by concretes B and C, for which the experimental data, characterized by low values of D/l_1 (below 2 in the CCL scale), are situated on the part of the CCL curve which substantially deviates from the asymptote. In this case their interpretation through the SEL is clearly not valid, and this explains the large discrepancies between the values of the parameters predicted by the two models.

The suitability of the SEL for the identification of the fracture parameters from experimental peak load data cannot be assessed *a priori* because it depends on the ratio of the specimen's depth to the characteristic length of the material, which, in turn, is an outcome of the parameter identification itself. For this reason one could be inclined to favor the CCL over the SEL.

This conclusion, however, is questionable in light of the unrealistically large values of G_f obtained for concretes B and C. For the CCL, this finding could be explained by the fact that with such low values of D/l_1, the inevitable scatter of test results could prevent the correct identification of the CCL asymptote. However, the predictions of the SEL, which give a lower bound for G_f, are also unrealistically high. Low D/l_1 values, then, do not provide adequate experimental results for the identification (through either SEL or CCL).

The explanation of this finding can be based on the observation that, for specimens having low D/l_1 values, the stresses in the FPZ belong to the pre-peak and immediately post-peak region of the stress–strain or stress–separation curve (Fig. 1). The pre-peak nonlinearities might be not negligible, because, although the energy corresponding to this stage is only 5% of the total fracture energy [5], it may represent a large fraction of the energy actually dissipated during loading up to the peak by specimens with low D/l_1 values. In addition, the initial tangent of the immediate post-peak of the softening curve, indicated by the measured structural strengths, might not correspond to the average slope of the curve (t_2 in Fig. 1b), but to a less inclined one, exemplified by tangent t_1 in Fig. 1b. This explanation would agree with the finding [25] that the size effect law may not be effective in determining the immediate post-peak shape of the softening curve.

4.6. Precision of the estimates

In the previous analysis, model parameters were identified using the average value of σ_N across experimental trials (typically three for each dimension D of the tested specimens).

In order to assess the influence of the variability of the experimental values of σ_N on the statistical accuracy of the parameters obtained with the optimization procedure, "bootstrap" resampling [26] of the original sets of test results was performed.

With this method, one thousand resampled data sets were generated by drawing with replacement from the sets of the σ_N values measured for each dimension D. Values of σ_N corresponding to different D were drawn independently from each other. The mean of the resampled values of σ_N corresponding to each D was used in the optimization, which was repeated for each of the 1000 bootstrap resamplings of the data, thus obtaining a new estimate of the fracture parameters for each set. This procedure allowed us to quantify the relationship between the typical variation in the experimental measures of σ_N and the resulting variations of the optimized parameters f_t and G_f, without making any assumption about the underlying distributions.

Due to the asymmetrical shape of the observed distributions of the optimized parameters (shown for concrete N in Fig. 10), we chose to report the median, the 15th percentile and the 85th percentile of each distribution, instead of the mean and standard deviation (the 15th percentile and the 85th percentile define an interval, positioned around the median, capturing 70% of the observed outcomes of the optimized parameters – analogous to mean ± standard deviation for a normal distribution).

The values of the medians and of the 15th and 85th percentiles which characterize the distributions of G_f and f_t predicted by the CCL and of G_f and c_f predicted by the SEL are reported in Tables 9 and 10, respectively. The values of the medians are very similar to the values obtained with the original set of data, while the values of the 15th and 85th percentiles show large percentage deviations relative to the medians. These deviations are comprised between −18% and +25% for G_f predicted by the SEL, between −28% and +49% for G_f predicted by the CCL, between −28% and +68% for f_t predicted by the CCL and between −47% and +66% for c_f predicted by the SEL.

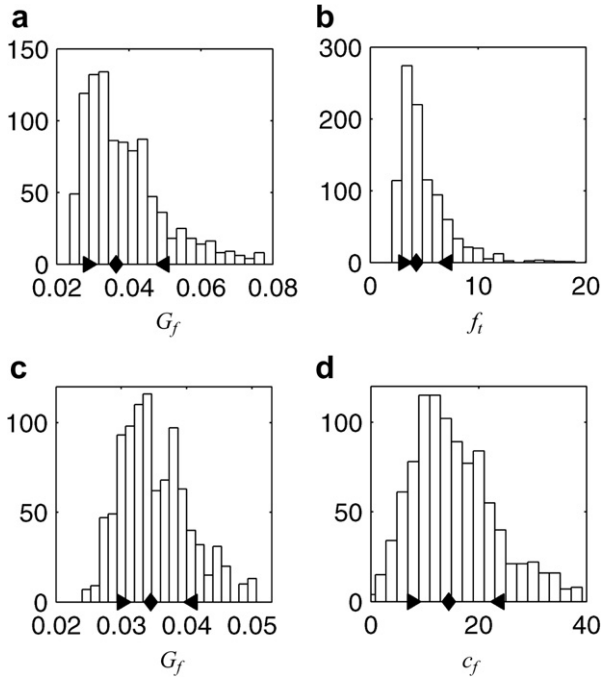

Fig. 10. Concrete N: histograms of the distributions of the optimized parameters across 1000 bootstrap resamplings of the original data sets. (a, b) CCL; (c, d) SEL. Diamonds: median values. Triangles: 15th and 85th percentiles.

Table 9
Median and percentiles values of the distributions of G_f and f_t predicted by the CCL

Concrete Mix	G_f^{15} (N/mm)	G_f^m (N/mm)	G_f^{85} (N/mm)	f_t^{15} (N/mm^2)	f_t^m (N/mm^2)	f_t^{85} (N/mm^2)
N	0.029	0.036	0.050	3.06	4.27	7.15
	(−21%)		(+37%)	(−28%)		(+68%)
S	0.040	0.048	0.060	3.93	4.79	5.98
	(−16%)		(+26%)	(−18%)		(+25%)
B	0.062	0.074	0.090	3.52	3.91	4.38
	(−16%)		(+22%)	(−10%)		(+12%)
C	0.112	0.156	0.233	2.69	3.05	3.48
	(−28%)		(+49%)	(−12%)		(+14%)

Superscripts: m, median; 15, 15th percentile; 85, 85th percentile.

Table 10
Median and percentiles values of the distributions of G_f and c_f predicted by the SEL

Concrete mix	G_f^{15} (N/mm)	G_f^m (N/mm)	G_f^{85} (N/mm)	c_f^{15} (mm)	c_f^m (mm)	c_f^{85} (mm)
N	0.030	0.034	0.041	7.7	14.4	23.9
	(−13%)		(+19%)	(−47%)		(+66%)
S	0.038	0.045	0.053	9.9	16.8	25.5
	(−15%)		(+19%)	(−41%)		(+52%)
B	0.052	0.059	0.067	21.8	28.3	35.6
	(−11%)		(+13%)	(−23%)		(+26%)
C	0.081	0.099	0.124	37.8	53.9	75.0
	(−18%)		(+25%)	(−30%)		(+39%)

Superscripts: m, median; 15, 15th percentile; 85, 85th percentile.

The precision of the estimates of G_f and f_t is better for the SEL than the CCL and, for both cases, no improvement was obtained when the tested specimens were four for each size D instead of three (concrete C).

5. Conclusions

From the analysis of the experimental and computational results presented in this paper the following conclusions can be drawn:

(a) The classical Bažant's size effect law (SEL) is equivalent to the asymptotic behavior predicted for large sizes by the cohesive crack model (CCL). Exploiting this equivalence it is possible to establish a unique relationship between the parameters of the SEL and of the CCL. Such relationship can be used either to compute the tensile strength from the identified SEL parameters or the equivalent crack extension from the identified CCL parameters.
(b) More specifically, through this relationship, it is possible to use the SEL not only for the identification of the initial fracture energy (as traditionally done) but also for the identification of tensile strength (Eq. (5)).
(c) The analysis of TPB experimental results shows that the two models are applicable only if the specimens are characterized by values of D/l_1 lying in the range 2–5 (on the CCL scale). For D/l_1 less than 2, not only the SEL asymptotic behavior cannot be captured, but also the CCL predictions appear unacceptable. For D/l_1 greater than 5, both models would depart from their range of validity because the stress profile in the FPZ cannot be predicted accurately by assuming a linear cohesive law.
(d) Because of item (c), there is not justification to favor the CCL over the SEL for the identification of G_f, and f_t. On the contrary, the SEL seems to be more appealing because it only requires a linear regression analysis and it accounts for the effect of specimen geometry and boundary conditions automatically.
(e) The variability of the fracture parameters predicted by the two methods as a function of typical variations of the experimental measures was assessed using "bootstrap" replications of the original test data. The results indicate that the precision of the estimates (of G_f, f_t, and c_f) obtained through the SEL is better than the one obtained through the CCL.

Acknowledgements

The authors are grateful to the students whose work for the master thesis provided an important part of the evidences presented in this paper. Special thanks to Professor Roberto Felicetti and to the Technicians Tonino Cocco and Paolo Broglia, who supervised the students in setting up the experimental apparatus. Special thanks to Leonardo Cedolin, who carried out the bootstrap analysis, and to the students Stefano Eccheli and Mario Roveda, who gave a great help in the preparation of this paper.

References

[1] Bažant ZP, Planas J. Fracture and size effect in concrete and other quasibrittle materials. Boca Raton and London: CRC Press; 1998.
[2] Hillerborg A, Modéer M, Petersson PE. Analysis of crack formation and crack growth in concrete by means of fracture mechanics and finite elements. Cement Concrete Res 1976;6:773–82.
[3] Planas J, Guinea GV, Elices M. Size effect and inverse analysis in concrete fracture. Int J Fracture 1999;95:367–78.
[4] Heilmann HG, Hilsdorf H, Finsterwalder K. Festigkeit und verformung von beton unter zugspannungen. Deustcher Ausshuss fur Stahlbeton 1969:203.
[5] Cedolin L, Dei Poli S, Iori I. Tensile behavior of concrete. ASCE J Eng Mech 1987;113(3):431–49.
[6] Guinea GV, Planas J, Elices M. Measurement of the fracture energy using three-point bend tests Part 1– Influence of experimental procedures. Mater Struct 1992;25:212–8.
[7] Planas J, Elices M. Asymptotic analysis of a cohesive crack. 2. Influence of the softening curve. Int J Fracture 1993;64:221–37.
[8] Guinea GV, Planas J, Elices M. Measurement of the fracture energy using three-point bend tests Part 3– Influence of cutting the P-d tail. Mater Struct 1992;25:327–34.
[9] Bažant ZP. Concrete fractures models: testing and practice. Eng Fract Mech 2002;69:165–205.
[10] Bažant ZP, Yu Q, Zi G. Choice of standard fracture test for concrete and its statistical evaluation. Int J Fract 2002;118:303–37.

[11] Cedolin L, Cusatis G. Cohesive fracture and size effect in concrete. In: Carpinteri A, Gambarova P, Ferro A, Plizzari GA, editors. Proceedings of the 6th int conf on fracture mechanics of concrete and concrete structures. London: Taylor and Francis; 2007.
[12] Bažant ZP. Size effect in blunt fracture: concrete, rock, metal. ASCE J Eng Mech 1984;110:518–35.
[13] Planas J, Guinea GV, Elices M. Generalized size effect equation for quasi-brittle materials. Fatigue Fract Eng Mater Struct 1997;20(5):671–87.
[14] Bažant ZP. Scaling of structural strength. London: Hermes-Penton Science; 2002.
[15] Carlucci A. Interaction between concrete fracture and bond (in Italian). Master Thesis, Politecnico di Milano University, 2003.
[16] Auriemma M, Avogadri M. Fracture properties of concrete (in Italian). Master Thesis, Politecnico di Milano University, 2005.
[17] Tada H, Paris PC, Irwin GR. The stress analysis of cracks handbook. Saint Louis (MO): Paris Productions; 1985.
[18] Taini, G. 2002. Experimental determination of fracture energy of concrete (in Italian). Master Thesis, Politecnico di MilanoUniversity; 2002.
[19] Barcillesi A, Baroni S. Experimental determination of fracture characteristics of concrete (in Italian). Master Thesis, Politecnico di Milano University; 2003.
[20] Colombo L. Analysis of fracture tests using the coesive crack model (in Italian). Master Thesis, Politecnico di Milano University; 2004.
[21] Cusatis G, Bažant ZP, Cedolin L. Confinement–shear lattice model for concrete damage in tension and compression. I: theory. ASCE J Eng Mech 2003;129(12):1439–48.
[22] Cusatis G, Bažant ZP, Cedolin L. Confinement–Shear lattice model for concrete damage in tension and compression. II. Numerical implementation and validation. ASCE J Eng Mech 2003;129(12):1449–58.
[23] Cusatis G, Bažant ZP, Cedolin L. Confinement–shear lattice model for fracture propagation in concrete. CMAME [special issue on Computational Modeling of Concrete] 2006:7154–71.
[24] Cusatis G, Cedolin L. Two-scale analysis of concrete fracturing behavior. Eng Fract Mech 2007;74:3–17.
[25] Guinea GV, Elices M, Planas J. Assessment of the tensile strength through size effect curves. Eng Fract Mech 2000;65:189–207.
[26] Efron B, Tibshirani RJ. An introduction to the bootstrap. New York: Chapman & Hall; 1993.